

## Supplementary Information

Simon I.R. Lane<sup>1,2</sup>, Jonathan Butement<sup>2,3</sup>, Jack Harrington<sup>3</sup>, Tim Underwood<sup>2,3</sup>, John Shrimpton<sup>1</sup> and Jonathan West<sup>2,3</sup>

<sup>1</sup>Faculty of Engineering and Physical Sciences, University of Southampton, UK.

<sup>2</sup>Institute for Life Sciences, University of Southampton, UK.

<sup>3</sup>Cancer Sciences, Faculty of Medicine, University of Southampton, UK.

### Sedimentation and Buoyancy Examples

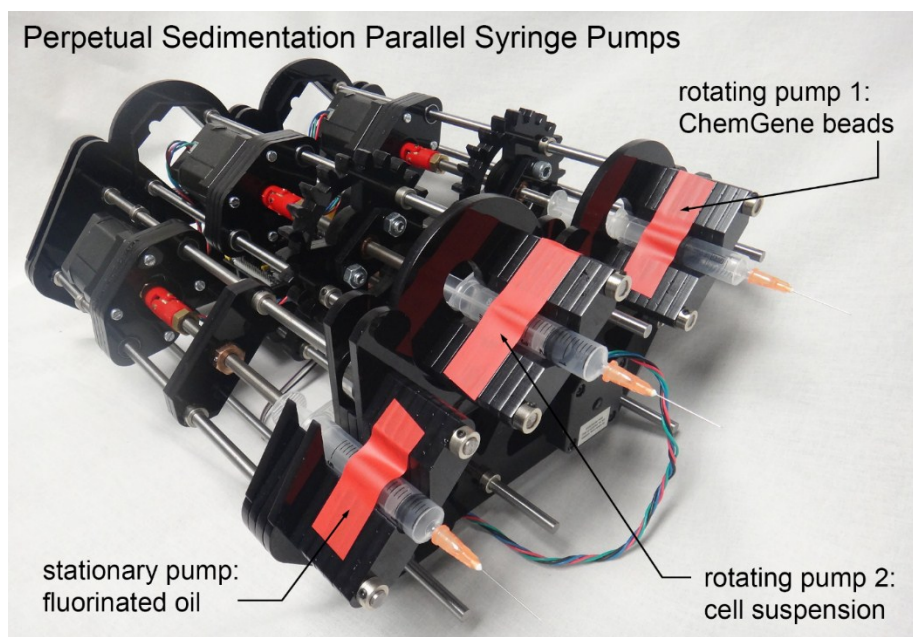
Illustration of the sedimentation and buoyancy velocities across a range of microfluidic scenarios calculated using  $U = (2(\rho_p - \rho_f)gR^2)/9\mu$ , where  $U$  is the sedimentation velocity,  $g$  is acceleration due to gravity and  $\mu$  the dynamic viscosity of the fluid. Syringe diameter and delivery duration are required to inform whether perpetual sedimentation is needed. For example, perpetual sedimentation is not required for a typical platelet experiment.

Object	Fluid	Diameter (μm)	Object density (kg/m <sup>3</sup> )	Fluid density (kg/m <sup>3</sup> )	Fluid Viscosity (N s/m <sup>2</sup> x 10 <sup>-3</sup> )	Velocity/Direction (mm/10 min)
Platelet	Aqueous	2.5	1050	1000	0.889	0.07 ↓
White blood cell	Aqueous	10	1050	1000	0.889	1.63 ↓
Human oocyte	Aqueous	100	1050	1000	0.889	163 ↓
Magnetic particle	Aqueous	3	~2000	1000	0.889	2.94 ↓
Magnetic particle	Aqueous	10	~2000	1000	0.889	32.7 ↓
Aqueous droplet	Fluoro-oil	10	1000	1850	3.400	8.17 ↑
Aqueous droplet	Fluoro-oil	100	1000	1850	3.400	817 ↑

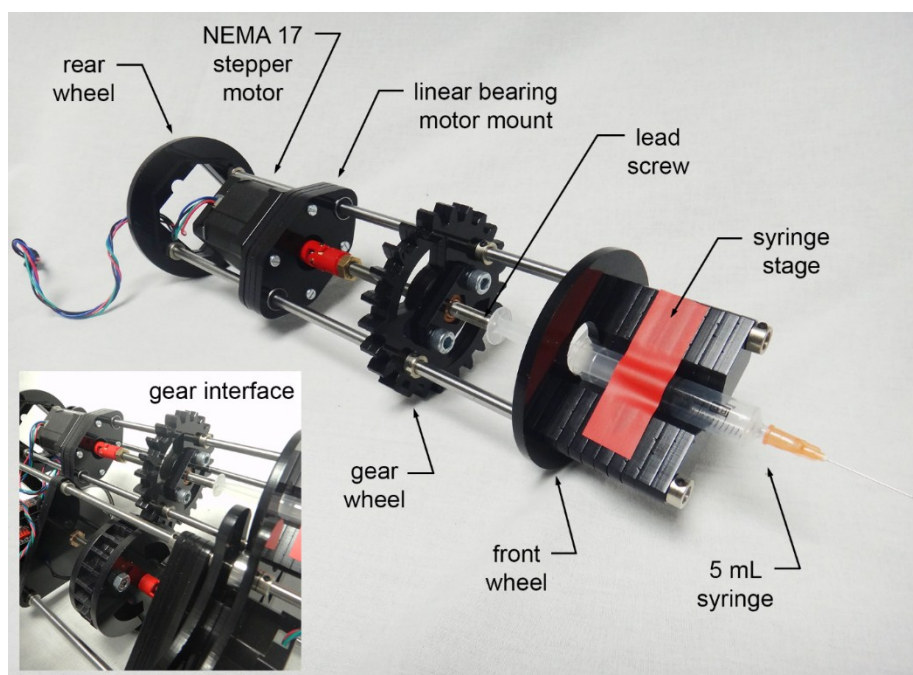
**Table.** Sedimentation and buoyancy rates for cells, particles and droplets. The fluoro-oil properties are those of Fluorinert™ FC-40. Room temperature (25°C) values are documented. Velocity units reflect a typical minimal processing time.

### Perpetual Sedimentation System

Comprehensive instructions, design files and operating code are available as a github repository<sup>1</sup>. In this work, a 60W CO<sub>2</sub> laser (Epilog Mini) was used to cut 5-mm-thick PMMA parts that were mounted on a frame of 6-mm-diameter, 333-mm-long silver steel rods. PMMA parts were secured in place using 6 mm zinc collets and M6 nuts and bolts. An 85-mm-diameter gear wheel with 24 teeth and 20° pressure angle, driven by a powerful NEMA17 stepper motor (54 N.cm holding torque), was used to rotate same-sized gear wheels on two syringe pumps. Reversal of the rotation direction every 360° was used to prevent cable and tubing entanglement. The syringe pumps have front and rear PMMA wheels that roll over ball bearings (two per wheel, 8x22x7 mm deep groove, Simply Bearings) mounted on the steel rods of the system chassis. Within each pump a precision lead screw (317 μm/rev linear motion) passes through a locking bushing nut within the gear wheel for displacement of the syringe plunger. The lead screws are also driven by NEMA17 stepper motors with actuation within the steel rod frame achieved by mounting on linear bearings. A RAMPS 1.4 controller board with an Arduino MEGA2560 (Ooznest Ltd) is used to relay instructions to stepper motor drivers (DRV8825, each limited to 1.2A). Precision stepping (0.795 μm/step) is combined with microstepping; 1/8 step for the gear motor and 1/16 step for the syringe pumps. The system is powered using a 12V 5A mains adaptor, with commands sent to the Arduino from a Graphical User Interface (GUI) developed using python for straightforward control (rpm, direction, syringe ID and flow rate, global stop). A three-pump system for Drop-seq microfluidics is shown in SI Fig. 1 along with a single rotating syringe pump in SI Fig. 2.



**SI Fig. 1.** A parallel syringe pump PS prototype supporting two rotating syringe pumps and a third static syringe pump. This system was designed for Drop-seq microfluidics involving the independent delivery of  $\sim 30\text{-}\mu\text{m}$ -diameter ChemGene transcriptome capture beads, a cell suspension and the fluorinated carrier oil for co-encapsulation in monodisperse droplets.

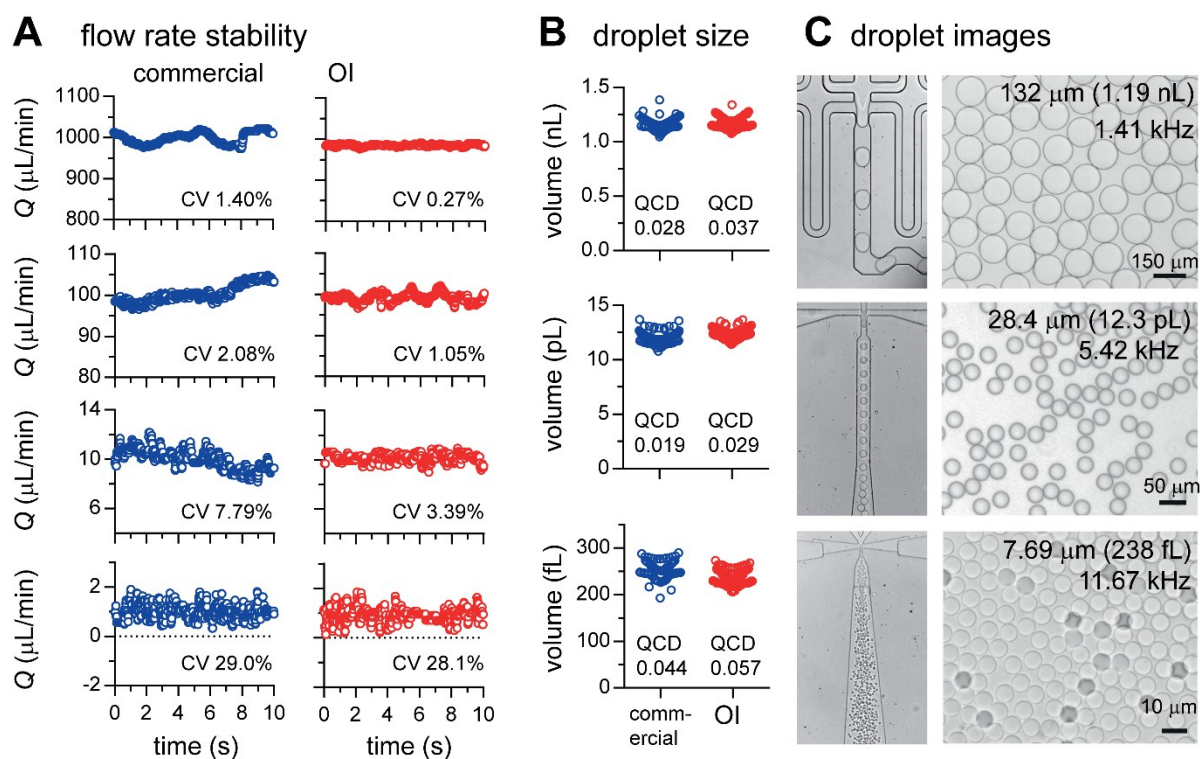


**SI Fig 2.** A rotating syringe pump with an image of the gear interface (inset).

## Open Instrumentation Syringe Pump Characterisation

Flow rate stability was measured by connecting commercial and open hardware syringe pumps via 80 mm PEEK tubing with Omnifit® 1/16" (Kinesis) interconnect to a 1 mm ID Flow Sensor (ElveFlow) with data acquisition using the OB1 Pressure Controller (Mk 3, ElveFlow). 100 Hz sampling for 10 s was used to obtain the traces. The syringe diameter and material, plastic or gas-tight glass, affect flow stability. Decadal flow rates were documented using 100  $\mu\text{L}$  (1 and 10  $\mu\text{L}/\text{min}$ ; 1.46 mm ID), 1 mL (100  $\mu\text{L}/\text{min}$ ; 4.61 mm ID) and 2.5 mL (1000  $\mu\text{L}/\text{min}$ ; 7.28 mm ID) gas tight glass syringes (SGE Analytical Science). The flow rate stability and scalable droplet generation results are

presented in SI Fig. 4. The back pressure tolerances of the pumps were measured using an in-line pressure sensor (FlowPlus16, ViscoTec) with Luer lock interfaces to the syringe and downstream to a 4-mm-long inertial focussing channel ( $w=30\text{ }\mu\text{m}$ ,  $h=65\text{ }\mu\text{m}$ ). A viscous ( $\sim 6.5\text{ cP}$ ) PEG3350 solution (50% (v/v)) was used as a challenging sample.

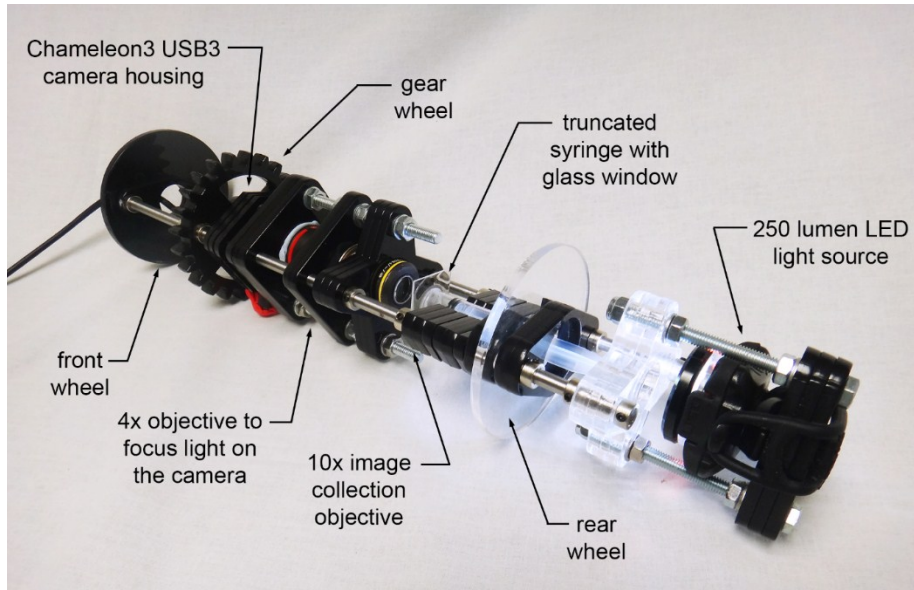


**SI Fig. 3:** Open instrumentation syringe pump characterisation and comparison with commercial grade systems (Fusion 200, Chemxy Inc.). (A) Decadal flow rate qualities using 100  $\mu\text{L}$ , 1 mL and 5 mL gas tight glass syringes (A). The precision lead screw produces higher stability flow rates. (B) Using commercial and open hardware syringe pumps monodisperse droplets can be generated (B). These range from nanolitre to femtolitre volumes (QCD; quartile coefficient of dispersion,  $n > 100$ ). Images of droplet generation and stored droplets (C);  $\sim 1\text{ nL}$  droplets were generated using the microfluidic circuits provided by Macosko *et al*<sup>2</sup>,  $\sim 12\text{ pL}$  droplets using devices designed by Martin Fischlechner<sup>3</sup>, and  $\sim 250\text{ fL}$  droplets using devices designed by Jung-Uk Shim<sup>4</sup>.

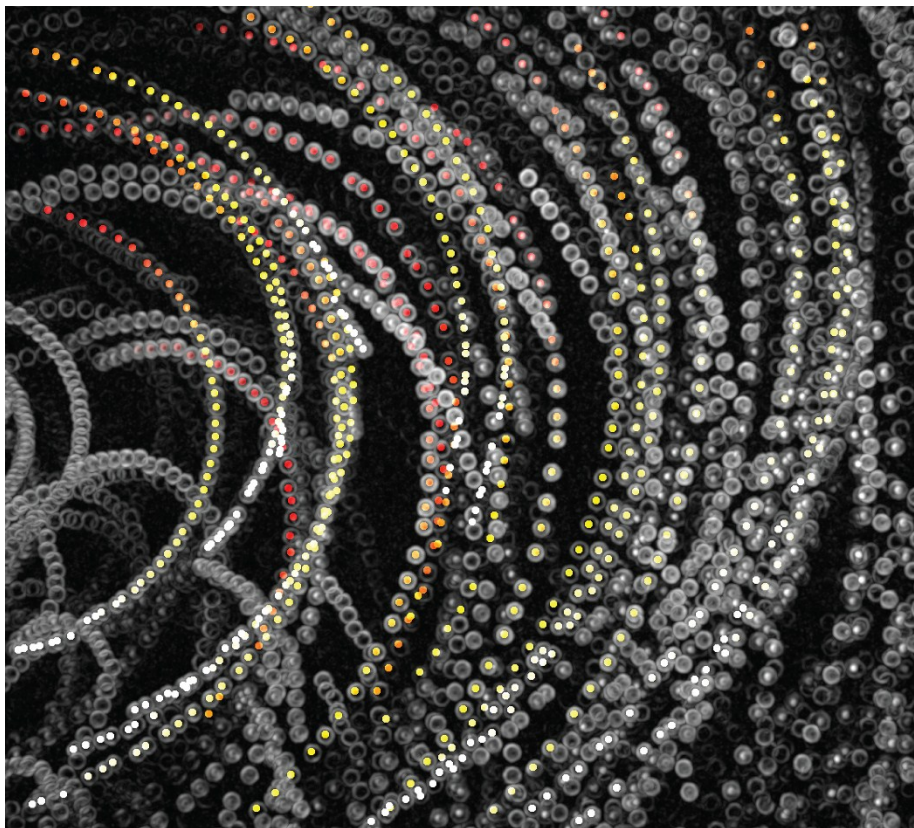
### Rotating Microscope Assembly and Orbit Analysis

To observe sedimentation during rotation a simple microscope was constructed and mounted on an axel for rotation (see SI Fig. 5). An opposing objective configuration was used, consisting of a 10x objective (Olympus, NA 0.30, WD 11.0 mm) for light collection from the sample and 4x objective (NA 0.13,  $\infty$ - WD 17.1 mm) for focusing light onto the CMOS camera (Chameleon3 USB3, Point Grey). A 250 lumen white LED bicycle light (Zecto, Lezyne) was used to illuminate a truncated syringe with a 1-mm-thick glass window to allow particles to be imaged. To attain steady state radial transport 10 rotations were used before reversal. The rotating microscope is shown in SI Fig. 4. A 50k/mL suspension of 30- $\mu\text{m}$ -diameter polystyrene particles in 1 x PBS with 0.1% Tween 20 was loaded into the syringe and imaged with rotation rates of 0.1–0.5 Hz (6–30 rpm) and compared with sedimentation without rotation. Mean and standard deviations of the orbit radii were obtained from 10–21 particles with 46–100 points measured for each complete orbit (see Figure 2B), with the mean and standard deviation of the net displacement velocity (see Figure 2C) measured from these orbits.





SI Fig. 4. Opposing objective microscope mounted between the wheels of the axle.



SI Fig. 5. Rotation with reversal every  $360^\circ$  introduces accelerations and decelerations to the radial velocity to prevent the accurate measurement of gravity-directed particle orbits. This example involved  $30\text{-}\mu\text{m}$ -diameter particles with a rotation frequency of 1 rpm.

### Microfabrication and Microfluidics

Soft lithography involving a SU-8 on silicon master was used to fabricate 95-mm-long Dean entrainment spirals (6 loops,  $R=1.66\text{--}3.16\text{ mm}$ ) in PDMS. The entrainment of  $30\text{-}\mu\text{m}$ -diameter particles involved a channel cross section

of 100 x 125  $\mu\text{m}$  (w x h), and for magnetic particles and cells a cross section of 50 x 50  $\mu\text{m}$ . A 1-mm-diameter biopsy punch (Miltex) was used to prepare inlet/outlet ports prior to oxygen plasma bonding (Femto, Diener Electronic) to a glass microscope. Fine bore polythene tubing (OD 1.09 mm; ID 0.38 mm; Smiths Medical) was directly inserted into the ports to securely interface the devices and was used to tightly sheath a 25G needle (BD) to interface with the syringe (5 mL; 12.07 mm ID, BD).

### Particle Suspensions, Actuation, Entrainment Imaging and Cell Viability

Particles (Kisker Biotech) were prepared in 1 x PBS solutions with 0.1% Tween 20 to reduce aggregation, and single cell suspensions were prepared in basal RPMI media (ThermoFisher Scientific). These samples were loaded into 5 mL syringes (BD) for microfluidic experiments. Dean entrainment was effected at 100 mm/s mean flow velocities (75  $\mu\text{L}/\text{min}$  for 30-micron particles ( $\kappa \approx 2.8$ ); 15  $\mu\text{L}/\text{min}$  for magnetic particles and cells ( $\kappa \approx 0.8$ )). Controls were without magnetic stirring or rotation, perpetual sedimentation involved syringe rotation and magnetic actuation used a Multi-Stirrus™ system with a 5-mm-diameter samarium cobalt stirring disc housed with the syringe (VP Scientific). The recommended level (25-30) was used for gently stirring ChemGene beads and cells. This approach does, however, fracture the ChemGene beads during prolonged actuation ( $\geq 20$  minutes) relevant to bead recycling or lengthy encapsulations (see Fig. 4(E)). An inverted microscope with 10x or 20x objective magnification was used to image 30 micron particle and magnetic particle and cell trains, respectively. Particulate trains were recorded at the spiral exit using a Miro Lab310 (Vision Research) high-speed camera (1000 fps, 10  $\mu\text{s}$  exposure). Time course experiments involved a 3 second (3000 frame) recording every minute. Triplicate experiments were used to derive the mean and standard deviation of the count rate and normalised to the first reading ('normalised delivery'). Cell viability was measured using a LIVE/DEAD® Viability/Cytotoxicity Kit (ThermoFisher Scientific) and analysed using an Attune NxT flow cytometer (ThermoFisher Scientific), with an unpaired t test used to calculate significance using data from 6 experimental replicates.

### Rotation Image Analysis

To measure perpetual sedimentation orbits during steady state syringe rotation ( $>3$  revolutions without direction change) recordings were made with frame rates between 5 and 50 fps and exposure times of 10 ms. The captured image stacks were processed in ImageJ (NIH) as follows: Stacks were truncated to a single revolution, reduced to 8-bit greyscale and inverted using the ImageJ math macro function: " $v=255-v$ ". The edge finding function and a Gaussian blur (sigma=2) were then applied to yield an image with a dark background and high contrast, suitable for automated particle tracing. The ImageJ plugin TrackMate v3.8.0<sup>5</sup> was then used to record particle positions using the LoG detector. Filters were applied to suppress edge artefacts. The "Simple LAP tracker" was then used to create traces from the particles over time. A filter was then applied to remove incomplete traces (moving out of focus), such that only traces where the particle was tracked over one complete revolution were used in further analysis. Orbit radii were calculated by finding the mean position of each trace, and calculating the distance from the mean position for each time point. Net displacement was calculated as the distance between the particle in the first and the last frame. To normalise for different rotational frequencies this is plotted as net displacement velocity. Heat map overlays were produced by feeding the x and y position from the tracking data into an in-lab ImageJ macro for colour coding using the Red Hot lookup table onto a time-projected image of the particles.

### References

1. <https://github.com/JohnnyJamesWest/Perpetual-Sedimentation>
2. E. Z. Macosko, A. Basu, R. Satija *et al*, *Cell*, 2015, **161**, 1202.
3. M. Fischlechner, Y. Schaerli, M. F. Mohamed *et al*, *Nature Chemistry*, 2014, **6**, 791.
4. J.-U. Shim, R. T. Ranasinghe, C. A. Smith *et al*, *ACS Nano*, 2013, **7**, 5955.
5. J.-Y. Tinevez, N. Perry, J. Schindelin *et al*, *Methods*, 2017, **115**, 80.